Lipid nanoemulsion incorporating DOTAP reverse micelles as clinically translatable carriers of ALDH inhibitors for lung cancer therapy

Maria Irujo[1], Laura Poussereau[1], Maïssam Ezziani[1]; Clotilde Joubertt[2], Chloé Prunier[2]; Julien Vollaire[3]; Véronique Josserand[3]; Cédric Sarazin[4], Daphna Fenel[5], Eleftherios Zarkadas[6], Mileidys Perez[1], Isabelle Texier[7], Alice Gaudin[1]

[1]Advanced BioDesign, 655 Allée des Parcs, France

[2]INOVOTION SAS, 38700 La Tronche, France

[3]IAB, OPTIMAL Small Animal Imaging Facility, 38000 Grenoble, France

[4]Nanoscale Metrix – L'Union, France

[5]Université Grenoble Alpes, CNRS, CEA, IBS, F-38000 Grenoble, France

[6]Université Grenoble Alpes, CNRS, CEA, EMBL, ISBG, F-38000 Grenoble, France

[7]Université Grenoble-Alpes, CEA-LETI DTIS, France

Corresponding author

Alice Gaudin, alice.gaudin@a-biodesign.com; Isabelle Texier, isabelle.texier-nogues@cea.fr

ABSTRACT

Lung cancer remains the most prevalent malignancy worldwide and the leading cause of cancer-related deaths. Bridging academic innovation and industrial applications is critical for developing scalable drug delivery systems for pulmonary therapies. In this study, we designed and optimized a lipid nanosystem incorporating the cationic lipid DOTAP by utilizing reverse micelle structures to enhance pulmonary tropism. Fluorescence quenching assays confirmed the incorporation of reverse micelles into the oily core, thus validating the structural integrity of the system. This nanosystem was tailored for the encapsulation of ABD0171, a potent inhibitor of ALDH1A3, an enzyme strongly associated with chemoresistance in lung cancer. Physicochemical characterization revealed robust colloidal properties with a particle size of 60 nm, surface charge of +45 mV, and encapsulation yield of 99%. *In vitro*, formulations with/without DOTAP demonstrated high efficacy against epithelial-like H358 cells derived from human bronchioalveolar carcinoma, with IC50 values < 5 µM. Chicken Chorioallantoic Membrane (CAM) evaluations demonstrated good tolerability of the DOTAP-containing

formulation and significant H358 tumor reduction by 28% compared with the untreated control, while maintaining a favorable safety profile. By combining industrially feasible methods with FDA-approved components, this study demonstrated the potential of DOTAP-containing lipid nanosystems as scalable platforms for pulmonary drug delivery. These findings provide a pathway for future applications in cancer therapy, bridging the gap between nanosystem innovation and clinical translation.

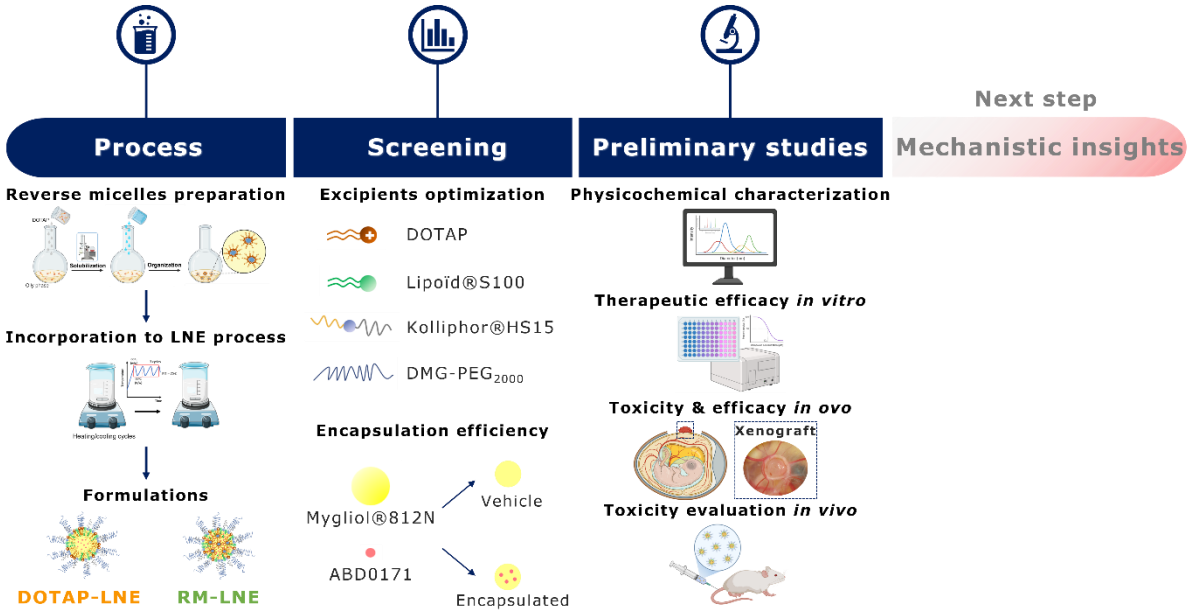

Graphical table of content

Keywords : Lipid nanocapsules, reverse micelles, pulmonary drug delivery, ALDH inhibitors, cancer therapy

1. INTRODUCTION

Lung cancer remains the most prevalent malignancy worldwide and is the leading cause of cancer-related deaths with 2.2 million new cases diagnosed annually [1,2]. Non-small cell lung cancer (NSCLC) accounts for approximately 80–85% of all lung cancer cases and includes adenocarcinoma, squamous cell carcinoma, and large cell carcinoma as the main histological subtypes [3]. Advances in screening techniques, such as low-dose computed tomography (LDCT), have improved early detection of the disease; however, most patients are still diagnosed at advanced stages, leading to poor prognosis [3,4]. As a result, the five-year survival rate for all stages combined remains as low as 28%, emphasizing the critical need for innovative therapeutic strategies [1,3]. Current therapeutic options for NSCLC include surgery, chemotherapy, radiotherapy, and targeted therapy. While targeted therapies and immunotherapies have demonstrated promising results, resistance to these treatments, as well as side effects, frequently emerge, driven by tumor heterogeneity and adaptive mechanisms, which significantly hamper their long-term effectiveness [1,2,5]. Consequently, there is an urgent need to develop novel therapeutic approaches to address these challenges and to improve patient outcomes.

One promising target in NSCLC therapy is the class 1 aldehyde dehydrogenase (ALDH) subfamily of enzymes, particularly the ALDH1A1 and ALDH1A3 isoforms, which has been shown to be implicated in tumorigenicity, chemoresistance, and disease progression [6–8]. ALDH1A3 has been identified as a biomarker of cancer stem-like cells and is associated with an enhanced tumor-initiating potential. Targeting ALDH1A3 sensitizes NSCLC cells to existing treatments such as chemotherapy and radiotherapy, potentially by amplifying reactive oxygen species (ROS) production [6]. However, the clinical translation of ALDH inhibitors (ALDHin) remains limited by their poor solubility, short plasma half-life, and rapid clearance *in vivo* [7]. This calls for the development of advanced nanocarrier systems to enhance ALDHin delivery and therapeutic use.

Lipid nanocarriers, including lipid nanoparticles (LNPs), lipid nanocapsules (LNCs), and lipid nanoemulsions (LNEs), have emerged as promising platforms for drug delivery. Their ability to encapsulate hydrophobic molecules, combined with their biocompatibility and potential for targeted delivery, make them ideal candidates for cancer therapy [9–11]. The incorporation of reverse micelles (RM) into these lipid nanosystems has further unlocked their capacity to encapsulate hydrophilic compounds, thereby overcoming one of the major challenges associated with conventional lipid formulations [12–14].

Despite these advances in the development of nanosystems with hybrid structures such as a combination of reverse micelles and lipid nanoemulsions, ensuring efficient delivery to the desired therapeutic site remains a critical challenge. Passive targeting, which relies on the enhanced permeability and retention (EPR) effect, often fails to bypass rapid clearance by the reticuloendothelial system (RES), significantly reducing circulation time [15]. Active targeting, on the other hand, involves functionalizing nanoparticle surfaces with specific ligands, and has shown promise in preclinical studies [11]. However, its large-scale translation is hindered by high production costs and limited clinical benefits [16]. An innovative approach to nanoparticle engineering is endogenous targeting, which exploits the interactions between the nanoparticle surface and plasma proteins for direct organ-specific delivery [17]. In particular, the incorporation of cationic lipids, such as DOTAP (1,2-dioleoyl-3-trimethylammonium-propane) into nanoparticle formulations has been shown to enhance lung tropism through a three-step mechanism: (a) desorption of polyethylene glycol (PEG) chains from the nanoparticle surface, (b) adsorption of plasma proteins onto the DOTAP-modified surface, and (c) subsequent recognition of these protein-nanoparticle complexes by adhesion molecule receptors specifically expressed in lung tissue [18]. Building upon this mechanism, and with a focus on clinical translation, our study explores the incorporation of DOTAP into lipid nanoemulsions as a strategy to facilitate pulmonary delivery of ABD0171, a potent and selective ALDH1A3 inhibitor [19].

In this study, we developed, optimized, and characterized a novel lipid nanoemulsion formulation incorporating DOTAP through reverse micelle structures (RM-LNE), constituting a stable and efficient colloidal drug delivery system capable of delivering ABD0171 to pulmonary cells, to unlock its therapeutic potential. During development, we assessed the physicochemical properties and therapeutic efficacy of three ABD0171-loaded formulations **(Figure 1)**: 1) LNE is a PEGylated version of the nanoemulsion developed by Heurtault et al. [20] incorporating DMPE-PEG2000, 2) DOTAP-LNE is the same formulation incorporating DOTAP by directly mixing it with the other LNE components, and 3) RM-LNE incorporates DOTAP as reverse micelles, to ensure the incorporation of DOTAP within the oily core and mimic the strategy developed by Dillard et al.(20), which suggested that the highest endogenous targeting behavior would be obtained in this setting.

This study demonstrates the potential of lipid nanoemulsions incorporating the cationic lipid DOTAP through reverse micelles structures as efficient and scalable nanocarriers for pulmonary drug delivery, showing robust physicochemical properties, high therapeutic efficacy

against the H358 NSCLC cell line (IC50 < 5 µM), and significant tumor reduction *in ovo* while maintaining a favorable safety profile.

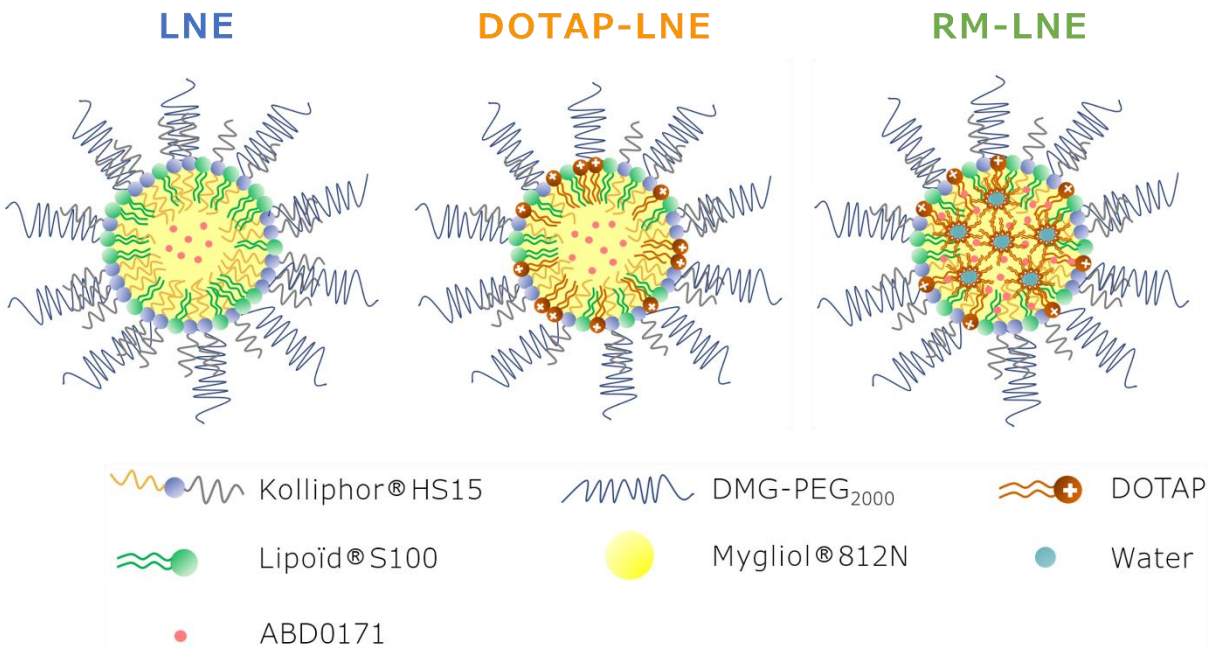

Figure 1: *Schematic representation of LNE (blue), DOTAP-LNE (orange), and RM-LNE (green) formulations: LNE (negative control without DOTAP), RM-LNE (DOTAP encapsulated as reverse micelles in the oily core), and DOTAP-LNE (DOTAP directly mixed with other components in a one-pot process).*

2. EXPERIMENTAL SECTION

2.1. Materials and reagents

The ALDH inhibitors (ALDHin) ABD0171 (2-Pentynethioic acid, 4-[[2-[(3,4-dimethylphenyl) methoxy] ethyl] methylamino]-4-methyl-, S-methyl ester) and DIMATE (4-dimethylamino-4-methyl-pent-2-ynthioic acid-S-methyl ester) were synthesized and characterized by Roowin SAS according to patents WO2001092220 and W02017064247. Kolliphor HS15 (Macrogol (15)-hydroxystearate) was purchased from BASF (Ludwigshafen, Germany), Mygliol 812N (triglycerides medium-chain) from IOI Oleochemical, Lipoïd S100 (soy lecithin with 100% phosphatidylcholine) and DOTAP (1,2-dioleoyl-3-trimethylammonium-propane chloride salt) were purchased from Lipoid GmbH (Ludwigshafen, Germany). CF (5(6)-Carboxyfluorescein) was purchased from Merck. DMPE-PEG2000 (N-(methylpolyoxyethylene oxycarbonyl)-1,2-

dimyristoyl-sn-glycero-3-phosphoethanolamine sodium salt) was purchased from NOF EUROPE GmbH (Frankfurt, Germany). Deionized water was obtained using a Milli-Q Plus system (Millipore, Paris, France). All the reagents and solvents used for chromatography were of analytical grade. Cell culture media, fetal bovine serum (FBS), and buffers were purchased from VWR (France). The NSCLC cell line, H358, was provided by the Institute of Advanced Biotechnologies, Grenoble (IAB). SYTOX Green and resazurin were purchased from Thermo Fisher Scientific

2.2. Preparation of Lipid NanoEmulsions (LNEs)

The detailed compositions of all the formulations are provided in the **Supporting Information (Table S1).**

The formulation of the lipid nanoemulsions (LNE) was adapted from the Phase Inversion Temperature (PIT) method reported by Garcion et al. [21]. Briefly, the aqueous phase components (Kolliphor HS15, Lipoïd S100, and 0.9% NaCl) were mixed and added to the oil phase containing Miglyol 812N, DMPE-PEG2000 and the ALDH inhibitor ABD0171. The mixture was heated to 90°C and then cooled to 60°C, during which the phase inversion temperature (PIT) is observed. This heating-cooling cycle was repeated twice two additional times to ensure system stabilization. At the end of the final cycle, the formulation is cooled to the PIT, and a large volume of cold water is added to stabilize the emulsion, a step refered as "quenching". The formulation was stirred for 10 min at room temperature and stored at 2–8°C until use.

Based on this fabrication process, three distinct LNE formulations and their associated preparation methods were developed and optimized. Each formulation was prepared with and without ABD0171 encapsulation, and the encapsulation efficiency was determined by the mass ratio of Miglyol to ABD0171 (8:1), yielding a final concentration around 15 mg/mL.

Standard LNE formulation (LNE)

The standard LNE formulation corresponds to the PEGylated nanoemulsion described above encapsulating ABD0171

DOTAP LNE formulation (DOTAP-LNE)

The DOTAP-LNE formulation was prepared using the same process as described for the standard LNE formulation, except that DOTAP was added to the oil phase before the addition of the aqueous phase, to obtain a DOTAP-incorporating nanoemulsion encapsulating ABD0171.

DOTAP reverse micelle LNE formulation (RM-LNE)

The reverse micelle LNE formulation incorporates the DOTAP lipid into the LNE core in a reverse-micelle (RM, water-in-oil) form. Briefly, initial solubilization was achieved by incubating DOTAP with Miglyol at 50°C under gentle stirring for 3 h. RM formation was obtained by adding water and stirring for 2 h. The formation of RMs was visually confirmed when a transparent, homogeneous, and stable solution was obtained. The lipid nanoemulsion was then prepared as a standard LNE formulation, except that during the final cooling step of the thermocycling process, the pre-formed RMs were added to the mixture to obtain a RM DOTAP-incorporating nanoemulsion encapsulating ABD0171.

2.3. Evaluation of reverse micelle formation using 5(6)-carboxyfluorescein encapsulation

To evaluate the formation of DOTAP reverse micelles (RM), 5(6)-carboxyfluorescein (CF) was encapsulated within the aqueous cores of ABD0171-RM-LNE. Briefly, CF was dissolved in water at a concentration of 50 mM, and 2–3 µL of 0.1 M NaOH was added prior to its incorporation into the DOTAP and Miglyol mix to form the RM. As a control, the same amount of CF was added at the final stage of ABD0171-DOTAP-LNE preparation (before the quenching step). CF fluorescence measurements were conducted in bulk formulations using a SpectraMax i3 plate reader (Molecular Devices, San Jose, CA, USA) with excitation at 450 nm, and emission spectra recorded from 475 to 800 nm in 2 nm increments. The samples were measured in black 96-well plates at 200 µL per well. To assess CF encapsulation, LNE formulations were disrupted by dilution in ethanol (1:2 v/v), followed by fluorescence measurement under the same conditions as the non-disrupted formulations diluted 1:2 v/v in MilliQ water.

2.4. Characterization of LNEs physicochemical properties

Measurement of size distribution and zeta potential by Dynamic Light Scattering (DLS)

The size distribution, polydispersity index (PDI), and zeta potential were measured using a Zetasizer Nano ZS instrument (Malvern Instruments, UK). Each formulation was diluted 1/100th in milliQ water before measurement. The material refractive index was set to 1.449, material absorption to 0, dispersant viscosity to 0.8872 cP, dispersant refractive index to 1.33, and dispersant dielectric constant to 78.5. Measurements were performed after a 100 s equilibration period at 25°C using a 173° backscatter angle. Three measurements were

performed, consisting of 10 runs of 10 seconds each. Particle size measurements were performed in a plastic cuvette, and zeta potential measurements were performed in DTS1070 measurement cells. The data were expressed as z-average values of particle size, determined by intensity distribution

Transmission Electron Microscopy (TEM) Imaging and Analysisanalysis

For cryo-TEM, 3.5 µL of each sample was applied to glow-discharged Quantifoil 300 mesh R1.2/1.3 or R2/2 grids in a Vitrobot Mark IV (Thermo Fisher Scientific) at 22 °C and 100% humidity. After 10 seconds of incubation, excess liquid was blotted from both sides for 2–5 seconds using a blot force of −7 or 0, and grids were plunge-frozen in liquid ethane.

Grids were screened on a Glacios Cryo-TEM (Thermo Fisher Scientific) at the Institut de Biologie Structurale (IBS), operated at 200 kV. Regions containing thin vitreous ice and well-distributed particles were selected for data collection. Cryo-EM datasets were acquired using the EPU automated acquisition software. Micrographs were recorded on a Falcon 4i direct electron detector at nominal magnifications of 73,000×, 150,000×, or 310,000×, corresponding to calibrated pixel sizes of 1.9 Å, 0.94 Å, and 0.46 Å, respectively. All micrographs were acquired with a total dose of approximately 34 $e^{-}/Å^2$ and defocus values between −2 and −3 µm.

Micrographs were analyzed using ImageJ for nanoparticle size measurements.

Quantification of ABD0171

Quantification of ABD0171 was performed using High-Performance Liquid Chromatography (HPLC) from Thermo Fisher (Ultimate 3000), with external calibration based on analytical standards. Calibration curve was established, and demonstrated linear responses ($R^2 > 0.99$) across the tested concentration ranges. Data analysis was conducted using Chromeleon software (Thermo Fisher, Waltham, MA, USA).

For ABD0171 quantification, analysis was performed using a Waters Symmetry C8 analytical column (4.6 × 50 mm, 3.5 µm) maintained at 40 °C, with a modified mobile phase composition. The mobile phase consisted of 10 mM ammonium acetate (phase A) and acetonitrile (phase B) in an isocratic ratio of 50:50 (v/v). The flow rate was set to 1.5 mL/min and UV detection was performed at 270 nm. The injection volume was 5 µL with a total run time of 10 min. The retention time for ABD0171 was 7.74 ± 1.0 min.

The extraction of ABD0171 from the formulations was performed by dissolving 140µL sample with 22.85mL acetonitrile, achieving a final dilution of 1:164. The resulting solution was transparent and 1mL transferred to separate HPLC vial.

Encapsulation efficiency of ALDHin in LNEs formulations by Taylor Dispersion Analysis

SD-TDA (Size Distribution - Taylor Dispersion Analysis) experiments were performed on a TaylorSizer instrument with a diode Array Detector from Nanoscale Metrix (Toulouse, France). UV measurements were performed at 200 and 270 nm. Bare-fused silica capillaries with inner diameter of 50 µm, a total length of 60 cm, and a length to detection window of 49.5 cm, were used for all experiments. The temperature of the capillary area was set to 25°C for the LNE formulations and 35°C for sample. The data processing was performed by TaylorSoft which included a patented algorithm enabling size distribution through SD-TDA. For the encapsulation measurements, the analyses were carried out at the specific wavelength of ABD0171 and the RM (270 and 200 nm, respectively), enabling relative quantification of the species present in solution.

***In vitro* release of ABD0171 from LNEs formulations**

The release of ABD0171 from the formulations was assessed by dialysis using Slide-A-Lyzer™ Dialysis Cassettes (Thermo Fisher, 10 kDa MWCO, 3 mL capacity). Following hydration of the membrane, 3 mL of the formulation were loaded into the dialysis cassette and immersed in 400 mL of 0.9% NaCl solution (release medium) under gentle stirring to maintain homogeneous conditions. The large volume of the release medium relative to the sample ensured the sink conditions throughout the experiment. After overnight incubation, the concentration of the retained drug in the dialysis cassette was quantified using previously described high-performance liquid chromatography (HPLC) methods.

Stability study of LNE formulations

The stability of the formulations was studied at 37°C, room temperature (RT), and 4°C. Each formulation was stored in glass vials, and at predetermined time points, the stability of the formulation was evaluated by measuring the physicochemical characteristics of the formulation by DLS (colloidal stability) and by quantifying drug degradation by HPLC (chemical stability).

2.5. *In vitro* evaluation

Cell line and culture conditions

H358 cells were cultured in RPMI 1640 medium supplemented with 1% L-glutamine, 1% penicillin/streptomycin, and 10% FBS unless otherwise specified. Cells were maintained in a humidified atmosphere containing 5% CO2 at 37°C.

Cytotoxicity assessment

The growth inhibitory effects of the formulations were evaluated using a resazurin-based cytotoxicity assay. H358 cells were seeded into 96-well plates at a density of 22,000 cells/cm^2 (7,000 cells/well) and incubated overnight at 37°C with 5% CO_2. For each evaluated formulation, cells were treated with a range of ALDHin concentrations (1 – 32 µM) and incubated at 37°C with 5% CO_2 for 48 h. Untreated cells (cell culture medium only) constituted the 100% viability control. A 20 µL volume of a 1X resazurin solution, prepared by diluting a 10X stock solution (1.5 mg/mL) in PBS, was added to each well and incubated for 3 h at 37°C. The fluorescence was measured (excitation: 560 nm; emission: 590 nm) using a SpectraMax i3 plate reader. The half-maximal inhibitory concentration (IC_{50}) was determined via non-linear regression analysis of log-dose/response curves using the GraphPad™ software. For each formulation, the experiment was repeated with N = 3 different formulations, with five biological replicates each time.

Cell viability assessment by flow cytometry (FACS)

Cell viability was assessed by flow cytometry based on membrane integrity loss using the SYTOX™ Green marker, which only penetrates dead cells with compromised membranes. H358 cells were seeded in 24-well plates at a density of 21,000 cells/cm^2 (40,000 cells/well) and incubated overnight at 37°C with 5% CO_2. For each evaluated formulation, cells were treated with ALDHin concentrations of 1.5 µM and 6 µM ALDHin for 2, 4, 6, and 24 h. At each time point, the medium was collected for dead cell recovery, and the cells were washed, detached with trypsin, and centrifuged at 180 × g for 5 min. The cell pellet was resuspended in PBS and stained with 5 µM SYTOX Green for 10 min in the dark. The fluorescence intensity was measured using a BD Accuri C6 Plus flow cytometer (Becton Dickinson) with excitation at 488 nm and emission at 585/40 nm (FL2 filter). The data were analyzed using the Kaluza™ software and expressed as the percentage of dead cells. For each formulation, the experiment was repeated for three different formulations.

2.6. *In vivo* evaluation

Toxicity studies in mice

The toxicity studies were conducted in collaboration with the Optimal Platform (La Tronche, France). All animal experiments were conducted in compliance with protocols approved by the Grenoble Ethics Committee and the French Ministry of Higher Education and Research (APAFIS#33137-2021110411585349v2). Forty-three six-week-old female NMRI nude mice (Janvier Labs, France) were used in this study. The details of the experimental groups and treatments are presented in **Table S1**.

Formulations were prepared by dilution in 0.9% NaCl and administered via tail vein intravenous injections (8 µL/g). To determine the maximum tolerated dose, body weight, behavior, and distress were monitored with euthanasia performed if ethical limits were exceeded. All the mice were euthanized for organ analysis at the end of the study.

Efficacy and toxicity study in the chicken CAM assay

According to French legislation, no ethical approval is required for experiments using oviparous embryos (Decree No. 2013–118, February 1, 2013; Article R-214-88). The chicken CAM assay was performed by Inovotion SAS (La Tronche, France) using fertilized White Leghorn eggs (Couvoir Hubert, France). The eggs were incubated at 37.5°C with 50% relative humidity for 9 days. On EDD9 (Embryonic Development Day 9), the chorioallantoic membrane (CAM) was dropped down by drilling a small hole into the air sac, followed by creating a 1 cm^2 window in the eggshell above the CAM. At least 15 embryos per group were used in the experiments.

The H358 tumor cell line was cultured in RPMI 1640 medium supplemented with 10% FBS, 1% sodium pyruvate, and 1% penicillin/streptomycin. On EDD9, H358 cells were detached using trypsin, washed in complete medium, and resuspended in graft medium. A total inoculum of 1×10^6 cells was applied onto the CAM of each egg, after which the eggs were returned to the incubator. Eggs were randomly divided into four treatment groups: negative control (0.9% NaCl), ABD0171 free compound, LNE, DOTAP-LNE, and RM-LNE. Treatments were administered at two doses of 2.76 mg/kg [10X] and 27.6 mg/kg [1X] by dropwise application onto the tumors on EDD11 and EDD13. The concentration of ABD0171 was determined based on *in vitro* IC50 values and *in vivo* toxicity results in mice. Egg survival was monitored daily until the end of the experiment. On EDD18, embryos were sacrificed, and the upper portion of the CAM containing the tumor was excised, washed with PBS, and fixed in 4%

paraformaldehyde (PFA) for 48 hours. Tumors were carefully separated from the surrounding CAM tissue and weighed to assess the average tumor weight in the experimental groups.

2.7. Statistical Analysis

For *in vitro* experiments, statistical comparisons between groups were performed using one-way ANOVA. Results were considered statistically significant at $p < 0.05$. Data are presented as mean ± standard deviation (SD). All statistical analyses were conducted using the GraphPad™ Prism software (version 10.4.1).

For the chicken CAM assay experiments, one-way ANOVA statistical analysis with post-tests was performed. Statistical differences between groups are indicated on graphs using a star notation system: *$0.05 \geq p > 0.01$, **$0.01 \geq p > 0.001$, *** $0.001 \geq p > 0.0001$ and **** $p \leq 0.0001$.

3. RESULTS AND DISCUSSION

Development and fluorescent confirmation of DOTAP reverse-micelles lipid nanoemulsions (RM-LNE)

The RM-LNE formulation was developed based on the solvent-free thermocycling method proposed by Heurtault et al. [20]. The selected composition of the formulation employs FDA-approved ingredients for parenteral administration, ensuring the safety and clinical translatability of the resulting formulation. To enhance pulmonary delivery, DOTAP was incorporated into the core of the nanoemulsion according to the strategy outlined by Dilliard et al. [18]. In contrast to Dilliard's microfluidic approach, we employed thermocycling, which requires the effective integration of DOTAP into the oily core of the nanoemulsion. Drawing from the work of Vrignaud et al., who demonstrated the incorporation of anionic dioctylsodium sulfosuccinate (AOT) micelles into lipid nanocapsules for peptide delivery [12,13,22], we investigated the formation of cationic reverse micelles. For example, Jörgensen et al. demonstrated that reverse micelles formed with didodecyldimethylammonium bromide, offer significant advantages over AOT-based formulations, including improved encapsulation efficiency, greater stability, enhanced bioavailability, and stronger membrane interactions [23].

The key steps in the manufacturing process of the RM-LNE formulation are illustrated in **Figure 2**, highlighting the optimization process parameters evaluated during formulation development. These parameters included the lipid concentration of the nanoemulsion, amount

of DOTAP in the reverse micelle structure, water-to-lipid ratio in the reverse micelle structure, and volume of reverse micelles added to the lipid nanoemulsion. The optimized process parameter optimization and formulation compositions are provided in the **Supplementary information (Figure S1).**

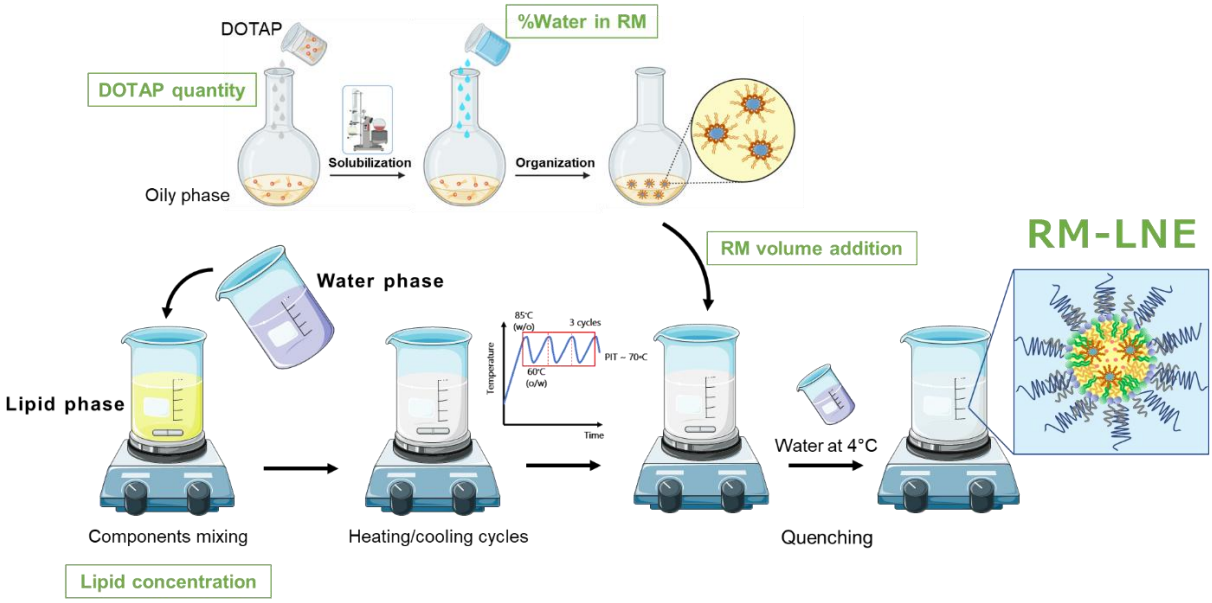

Figure 2: *Scheme illustrating the key steps in the preparation of DOTAP reverse-micelle lipid nanoemulsions (DOTAP-RM-LNE), with the optimized process parameters highlighted in green. The optimization focused on the DOTAP content in the RM structure, water percentage within the RM, and volume of RM added to the LNE formulation. DOTAP-RM-LNE formulations were fabricated using a thermocycling process, with reverse micelles (RMs) incorporated during the final temperature cycle.*

The formation of RM was verified by DLS, which provided insights into their size distribution, polydispersity, and stability. The data confirmed the formation of RMs with a monodisperse size distribution and a mean diameter of 14 nm (**Supplementary Information Figure S2**), which is consistent with previous reports on RM characterization [24].

To investigate the effective incorporation of RM into LNEs, we used 5(6)-carboxyfluorescein (CF), a hydrophilic dye commonly used as a fluorescent tracer in nanoparticle systems. CF is widely recognized for its ability to self-quench at high concentrations, a property attributed to dimerization and energy transfer mechanisms, making it a reliable marker for encapsulation studies [25]. Its application in various nanoparticle systems, including liposomes and reverse micelles, validates its suitability for evaluating our encapsulation strategy [12,26]. CF was incorporated into the aqueous core of RM during reverse micelles preparation and the resulting

RM(CF) were incorporated into the LNE formulation to form RM(CF)-LNE. The encapsulation of CF within the RM aqueous core was assessed by comparing the fluorescence intensity of the RM(CF)-LNE formulations with that of a control formulation, where CF was directly incorporated to the LNE formulation at the end of the thermocycling process (DOTAP-(CF)-LNE). In this control, CF was expected to reside in the aqueous dispersant phase and not in the oily core of the LNE (**Figure 2A).**

The fluorescence spectra of the RM(CF)-LNE formulations exhibited a consistent spectral profile across all samples (no shift in the emission wavelength), suggesting homogeneity in the CF distribution, as shown in **Figure 3B**. The corresponding fluorescence spectrum of RM(CF) is provided in **Supplementary Information Figure S3**, demonstrating that incorporation into the LNE did not affect the fluorescence properties of the RM(CF). As shown in **Figure 3C**, the significantly lower fluorescence intensity observed in the RM(CF)-LNE formulation compared to the DOTAP-(CF)-LNE formulation confirmed the self-quenching of CF within the RM cores, suggesting the successful encapsulation of RM in the oily core of the nanoemulsion. This finding is consistent with previous studies showing that reverse micelles can effectively encapsulate hydrophilic molecules, enabling controlled release and enhanced stability [26]. To further validate encapsulation, we disrupted the structure of both RM(CF)-LNE and DOTAP-(CF)-LNE formulations with ethanol, releasing CF into the dispersed medium (**Figure 3A)**. As shown in **Figure 3C**, RM (CF)-LNE fluorescence increased after disruption and was no longer significantly different from the fluorescence of DOTAP-(CF)-LNE, whose fluorescence slightly increases after disruption may be due to better solubilization by the solvent. This result confirmed that the same amount of CF was present in both systems, but encapsulated in different locations: encapsulated within the RM in the DOTAP-RM(CF)-LNE formulation *vs* free in the surrounding aqueous phase in the control formulation. These findings validated the successful incorporation of CF into the oily core of LNEs via DOTAP reverse micelles. This approach not only highlights the robustness of RM formation and their integration into LNEs but also underscores the potential of this platform for advanced drug delivery applications.

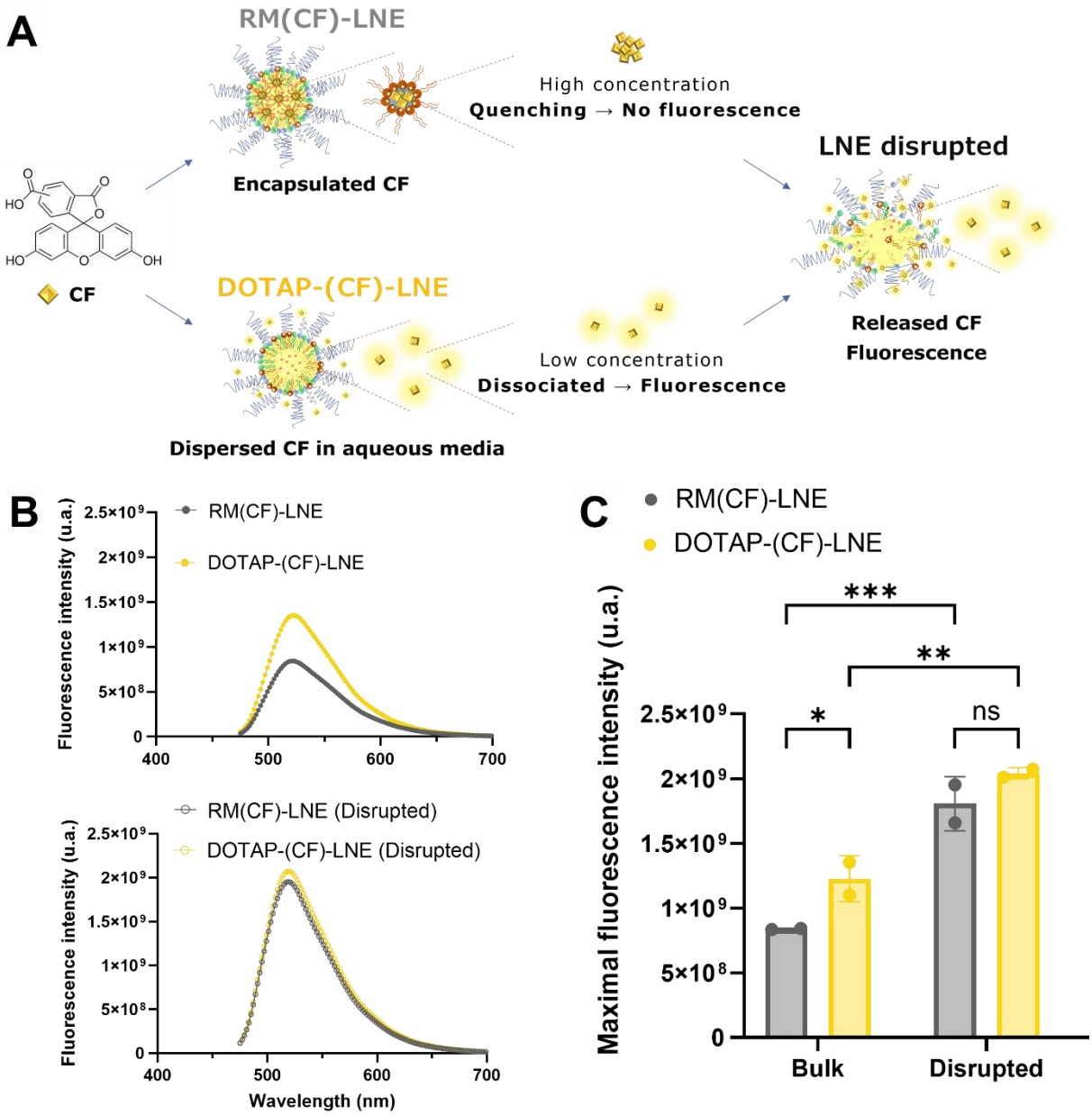

Figure 3: Reverse micelle encapsulation assay using CF and fluorescence analysis. (A) *Development of a reverse micelle encapsulation assay using 5(6)-carboxyfluorescein (CF). RM(CF)-LNE constitutes the formulation with DOTAP reverse micelles encapsulating CF, whereas DOTAP-(CF)-LNE includes DOTAP and CF directly added to the other components without the RM structure.* ***(B)*** *Fluorescence intensity spectra of RM(CF)-LNE and DOTAP-(CF)-LNE formulations in the bulk form and after disruption with ethanol.* ***(C)*** *Maximal fluorescence intensity of RM(CF)-LNE and DOTAP-(CF)-LNE formulations in the bulk form and after disruption with ethanol. Data represents the means of two independently prepared formulations (N=2) for each formulation. Statistical analysis was performed using two-way*

*ANOVA assuming a Gaussian distribution (*0.05, ≥ p > 0.01; **0.01, ≥ p > 0.001; *** 0.001, ≥ p > 0.0001).*

Development and characterization of LNEs

Lipid nanoemulsions (LNEs) are versatile delivery systems that are used to encapsulate lipophilic drugs with high efficiency. In this study, we evaluated the development of different LNEs optimized for encapsulation of ABD0171, a second-generation ALDH inhibitor with anticancer properties. Three formulations were optimized: LNE, DOTAP-LNE, and RM-LNE. The simplified LNE formulation was selected as a baseline to evaluate the impact of DOTAP on drug encapsulation and targeting efficiency, while offering a straightforward, well-established platform for drug delivery. The hypothesized structures of these formulations, including the localization of DOTAP, are illustrated in **Figure 1** along with the commercial names of their components. The detailed mass composition of each formulation is presented in **Table S2 of the Supplementary Information.**

Size measurement by DLS **(Figure 4A)** revealed that incorporating ABD0171 significantly increased the particle size in the DOTAP-LNE formulation from approximately 50 nm to 70 nm. On the other hand, the RM-LNE formulation as a vehicle (without encapsulated ABD0171) demonstrated a higher diameter compared to its counterpart LNE and DOTAP-LNE, and drug encapsulation did not induce any significant increase in diameter. These observations can be attributed to the hypothesis that, unlike RM-LNE, for which DOTAP was incorporated in the oily core, DOTAP in the DOTAP-LNE formulation was predominantly located at the surface of the LNE. Incorporation of RM in the oily core of the LNE induced an increase in diameter independent of drug encapsulation, whereas localization of DOTAP at the surface favored its interaction with Kolliphor HS15, causing a more pronounced increase in particle size upon drug encapsulation [27,28]. In particular, the larger polar head of DOTAP increased the effective head group area (a_0), reducing the packaging parameter (P), and consequently increasing the curvature radius and thus the particle size following drug encapsulation [29,30]. To be noted that all formulations exhibited PDI values below 0.15, confirming monodispersity and demonstrating that drug encapsulation did not compromise size distribution or induce aggregation.

These size trends were also confirmed by cryo-TEM imaging (Figure 4B–D), which revealed well-defined, monodisperse populations of spherical nanoparticles for all formulations, in agreement with DLS data. The measured sizes by TEM closely matched the DLS values, further

confirming the successful formation of a single-size population around ~60 nm. No aggregates or secondary populations were observed, supporting the low PDI values (< 0.15) obtained by DLS **(Figure 4A)**. Furthermore, close-up images (right panels) clearly show a distinct lipid shell surrounding the oily core (indicated by white arrows), highlighting the structural integrity of the nanoemulsion. Interestingly, no notable morphological differences were observed between the DOTAP-LNE and RM-LNE formulations, despite their differing methods of DOTAP incorporation (surface-localized vs. reverse micelle strategy). In particular, no micelle-like structures could be visualized within the lipid core of RM-LNE, suggesting either their disassembly or integration into the matrix below the resolution threshold of conventional cryo-TEM. To further investigate the internal organization of our nanoemulsions, advanced imaging techniques such as cryo-electron tomography (cryo-ET), known to reconstruct 3D nanoparticle architecture from tilt-series data [31], could provide definitive evidence of compartmentalization or hidden reverse micelles within the oily core.

Zeta potential (ZP) measurements **(Figure 4A)** indicated a stable positive surface charge (+45 mV) for both DOTAP-LNE and RM-LNE, regardless of DOTAP localization. This observation suggests that while increasing the DOTAP content in the formulation resulted in a larger particle size, it did not proportionally elevate the surface charge, likely due to charge saturation at the interface. **(Figure S4 in the supplementary information).** These findings align with studies showing charge density saturation at the nanoparticle surface, where additional charged components did not further increase ZP [32,33]. In contrast, lipid nanoparticles (LNPs) used for mRNA delivery typically exhibit neutral ZP values owing to charge neutralization by negatively charged mRNA [34,35]. The absence of this neutralizing effect in our formulations accounted for the positive ZP observed.

In summary, the distinct positioning of DOTAP significantly affected the nanoparticle size, likely through its interactions with Kolliphor HS15, while the observed charge behavior reflected a saturation effect. These results provide valuable insights into the structural and electrostatic factors influencing the design and stability of functional LNEs.

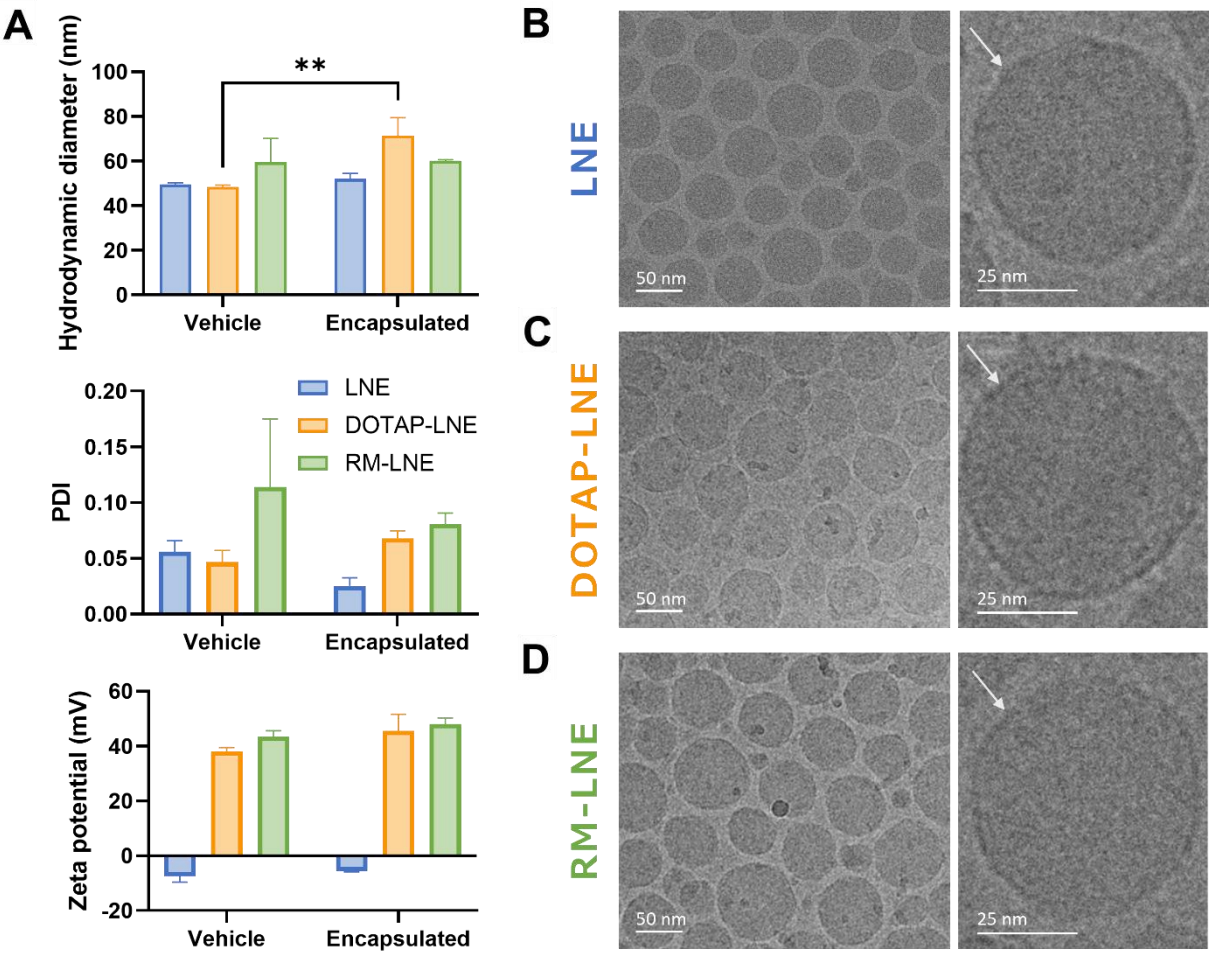

Figure 4: Physicochemical comparison of LNE, DOTAP-LNE, and DOTAP-RM-LNE formulations with and without ABD0171 encapsulation. *(A) Physicochemical characteristics of formulations, including hydrodynamic diameter (nm), polydispersity index (PDI), and zeta potential (mV), as determined by dynamic light scattering (DLS). Data are expressed as the mean ± standard deviation (SD) from three independent measurements (n=3). (B-D) Representative cryo-TEM images of ABD0171-loaded formulations: (B) LNE, (C) DOTAP-LNE, and (D) RM-LNE. Left panels show overview images; right panels display high-resolution views of individual nanoemulsion droplets. White arrows indicate the lipid shell surrounding the nanocarriers.*

Encapsulation yield and encapsulation efficiency of ALDHin in lipid nanoemulsions (LNEs)

Encapsulation yield and efficiency are critical parameters that influence the performance of lipid-based drug delivery systems. Encapsulation yield refers to the final quantity of drug in the

formulation compared to the initial amount of drug, translating the efficacy of the fabrication process to avoid drug loss. On the other hand, encapsulation efficiency aims to evaluate if the drug is properly encapsulated within the nanostructure of the drug delivery system, and not only dispersed it the surrounding media.

The encapsulation yields of the optimized formulations (LNE, DOTAP-LNE, and RM-LNE) were assessed using HPLC. All formulations encapsulating ABD-0171 exhibited near-complete encapsulation, with yields approaching 100% **(Figure 5B).** This high efficiency is likely attributable to the compound's physicochemical properties, particularly its high lipophilicity, as reflected by its predicted logP value **(Figure 5A)**.

To assess the encapsulation efficiency, Taylor Dispersion Analysis (TDA) was performed to evaluate the distribution of the drug between the free and nanoemulsion forms in all formulations. As shown in **Figure 5C** and **5D**, all optimized LNEs exhibited 100% encapsulation efficiency, with the drug fully incorporated into the lipid core. These findings contrast with previous observations by Roger et al. [36], who reported the persistence of residual micellar structures in lipid nanocapsule dispersions. Using transmission electron microscopy (TEM) and dynamic light scattering (DLS), their study highlighted the ability of Kolliphor HS15 to form stable micelles even after nanoemulsion formation. However, this behavior does not appear to affect the encapsulation of ABD-0171, likely due to its strong lipid affinity, which favors partitioning into the oily core over the aqueous phase or the surfactant micelles. Furthermore supporting these findings, Roger et al. [36] discussed how surfactant hydration and lipid interactions influence encapsulation, noting that surfactants such as Kolliphor HS15 can encapsulate drugs in micellar structures. Additionally, Yeging et al. [37] emphasized the role of lipid-surfactant interactions in determining the size and distribution of nanocapsules, which ultimately impact the encapsulation efficiency and release profiles.. This study applying SD-TDA measurements provide valuable insights into their encapsulation profiles and support their potential for efficient drug delivery.

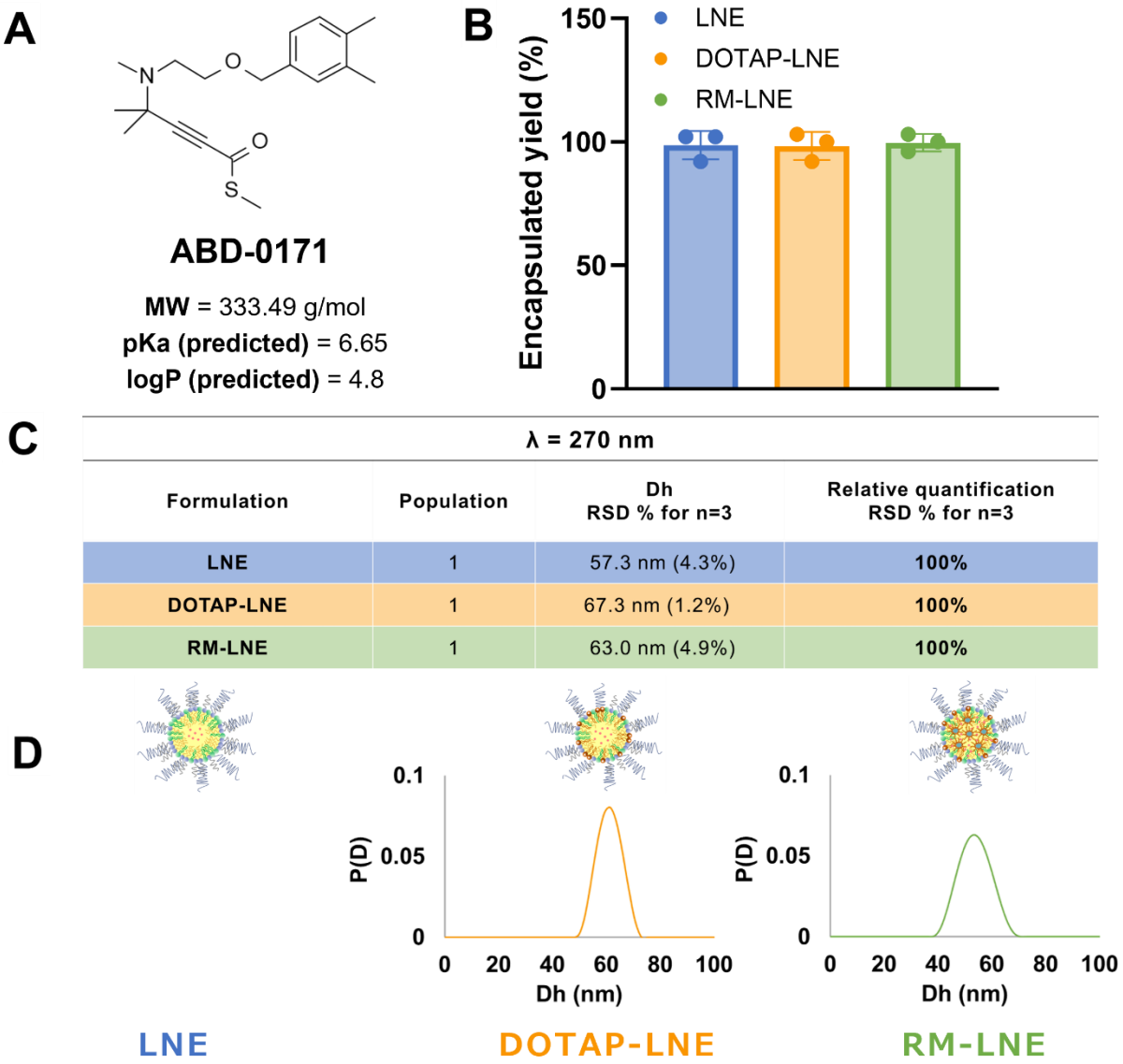

Formulation	Population	Dh RSD % for n=3	Relative quantification RSD % for n=3
LNE	1	57.3 nm (4.3%)	100%
DOTAP-LNE	1	67.3 nm (1.2%)	100%
RM-LNE	1	63.0 nm (4.9%)	100%

Figure 5: Encapsulation performances of ABD-0171 in LNE formulations. (A) *Chemical structures of ABD-0171, highlighting key physicochemical properties, such as molecular weight, pKa, and log P, relevant to this formulation and biological activity. (B) Encapsulation yield (%) of ABD-0171 in LNE (blue), DOTAP-LNE (orange), and RM-LNE (green) formulations (mean ± SD, n = 3).* ***(C)*** *Population distribution of ABD-0171 in each formulation, as determined by TDA.* ***(D)*** *TDA spectral profiles of LNE, DOTAP-LNE and RM-LNE,*

In vitro release and long-term stability of ABD0171 in nanoemulsions

The drug release profiles of the optimized formulations were evaluated by dialysis for 24 h. As shown in **Figure 6A**, ABD0171 was largely retained in the lipid core of all nanoemulsions, with minimal release observed after 24 h. The high lipid affinity of ABD0171, preferentially

associates with the lipid core of the nanoemulsions, leading to better retention and slower release. This is in accordance with the SD-TDA results (**Figure 5B and C**), which showed that 100% of ABD0171 was effectively encapsulated in the oily core of the nanoemulsion. These findings are consistent with those of previous studies demonstrating how the chemical properties of drugs influence their distribution within lipid nanoparticles. For example, Knoke et al. observed that lipophilic drugs are preferentially localized within the lipid core of nanoemulsions, where they are more stably retained, whereas hydrophilic drugs are more likely to migrate toward the aqueous phase, resulting in faster release profiles [38]. Similarly, the structural insights provided by Spinozzi et al. further confirm that the internal organization of lipid nanoparticles is directly influenced by the lipophilicity of the incorporated compounds, which dictates their localization and retention [39].

The stability of the formulations was further evaluated after 12 months of storage at 4°C. As shown in **Figure 6B**, the chemical stability of ABD0171 was preserved across all formulations, with only minor losses (< 5%) observed after 12 months. Dynamic Light Scattering (DLS) analysis (**Figure 6C**) confirmed the colloidal stability of all formulations, with no evolution in size distribution and a PDI consistently below 0.15, indicating that all nanoemulsions remained stable during the storage period **(Table S4 in supporting information)**. These results align with those of Danaei et al., who emphasized the critical role of particle size and polydispersity index (PDI) in determining the stability of lipid-based nanoparticles. A low PDI, as observed in our formulations, is essential for maintaining colloidal stability, ensuring uniform particle size, and minimizing aggregation during prolonged storage [40]. The consistent colloidal properties observed in our study further reinforce the robustness of the formulations under storage conditions, even for storage periods as long as 12 months, which is necessary for clinical translation.

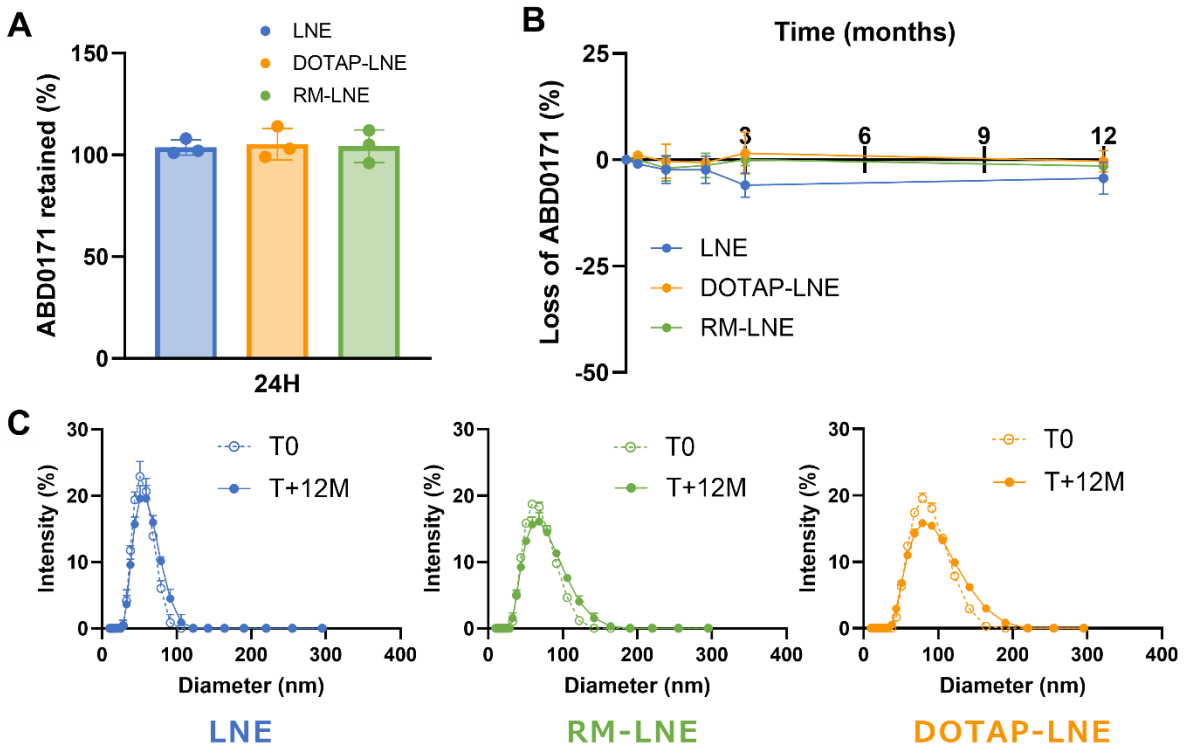

Figure 6: Stability assessment of ABD0171 in LNE formulations: retention, chemical, and colloidal stability. ***(A)*** *Retention percentages of ABD0171 after 24 h of dialysis.* ***(B)*** *Chemical stability of ABD0171 at 4°C for a 12-month period, as quantified by HPLC.* ***(C)*** *Colloidal stability of the nanoemulsions after 12 months of storage at 4°C, assessed by size distribution measurements using DLS.*

In vitro evaluation of therapeutic efficacy and safety of ABD0171 LNE formulations

To demonstrate the therapeutic potential of our approach for lung cancer treatment, we first assessed the *in vitro* efficacy of ABD0171 encapsulated in optimized lipid nanoemulsions (LNE, DOTAP-LNE, and RM-LNE) in H358 NSCLC cells using a resazurin assay. The IC50 values (**Figure 7A and 7B**) for all formulations were consistently below 5 µM, regardless of the zeta potential or composition of the formulation. These results suggest strong therapeutic potential, as IC50 values below 5 µM are typically indicative of highly promising anticancer agents [41,42]. To further evaluate the efficacy of the formulations, we assessed the cell death profiles using flow cytometry and SYTOX staining. **Figure 7C** displays the histogram of SYTOX-positive (SYTOX+) cell populations, which provides the quantification of dead cells expressed as a percentage of the total population. This analysis provides complementary insights into the IC50 values by offering a direct measure of cell death. Additionally, the kinetics of cell death overtime were monitored and are presented in **Figure 7D**, where the

percentage of dead cells is plotted as a function of treatment concentration and time. Notably, a marked increase in cell death was observed over time at a concentration of 6 μM compared to at 1.5 μM, for which the cell death population remained stable and low (<10%) throughout the observation period. These findings highlight the concentration-dependent nature of the cytotoxic effects and the time-dependent effect at a dose above the efficacious dose, which were consistent across all formulations tested.

To assess the safety profiles of the formulations, IC50 tests were conducted using empty vehicles (nanoemulsions without the active compound). Interestingly, the viability curves (**Figure 7A**) for the empty formulations revealed cell viability exceeding 100%, suggesting that lipid-based nanoemulsions could enhance cell metabolism. This phenomenon can be attributed to the unique properties of lipid nanoparticles, which are known to interact with cellular membranes and enrich them with lipid substrates that can be utilized for energy production and biosynthetic pathways, as previously reported [43,44]. Additionally, lipid nanoparticles have been shown to modulate metabolic activity by providing essential components for membrane synthesis and energy metabolism, particularly in metabolically active cells such as cancer cells [45]. These findings align with our observations, emphasizing that lipid-based nanoemulsions, in the absence of an encapsulated active pharmaceutical ingredient, can influence cellular behavior through metabolic support mechanisms.

Despite the presence of a positive charge on the surface of the DOTAP-containing formulations (DOTAP-LNE and DOTAP-RM-LNE), the observed lack of significant toxicity *in vitro* for the formulations without the drug (**Figure 7A**) suggests that the positive charge does not necessarily result in cellular toxicity. This finding aligns with the existing literature, which highlights that while positive charges on nanoparticle surfaces can enhance cellular uptake, they do not automatically lead to toxic effects. For example, Sharma et al. [42] indicated that while cationic nanoparticles may activate the complement system and induce toxicity, these effects are influenced by factors such as particle composition, biodegradability, and dose rather than being driven only by surface charge. Similarly, Goldstein et al. [41] emphasized that nanoparticle charge alone is not always predictive of drug efficacy or toxicity; instead, the interactions between the drug, delivery system, and cellular environment are pivotal in determining overall outcomes. Furthermore, studies on biodegradable nanoparticles have shown that adjusting surface properties, including charge, can reduce systemic toxicity by improving nanoparticle clearance, enhancing uptake by targeted cells, and minimizing immune system activation. In this regard, Salatin et al. [46] reported that surface charge, size, and shape are critical factors

affecting both cellular uptake and the reduction of toxic effects. Despite their cationic nature, our lipid-based formulations benefit from biocompatible lipid components and optimized design, which include biodegradable properties, thus minimizing toxicity. As a result, these formulations did not induce significant adverse cytotoxicity *in vitro*, supporting their potential as safe and effective drug delivery systems.

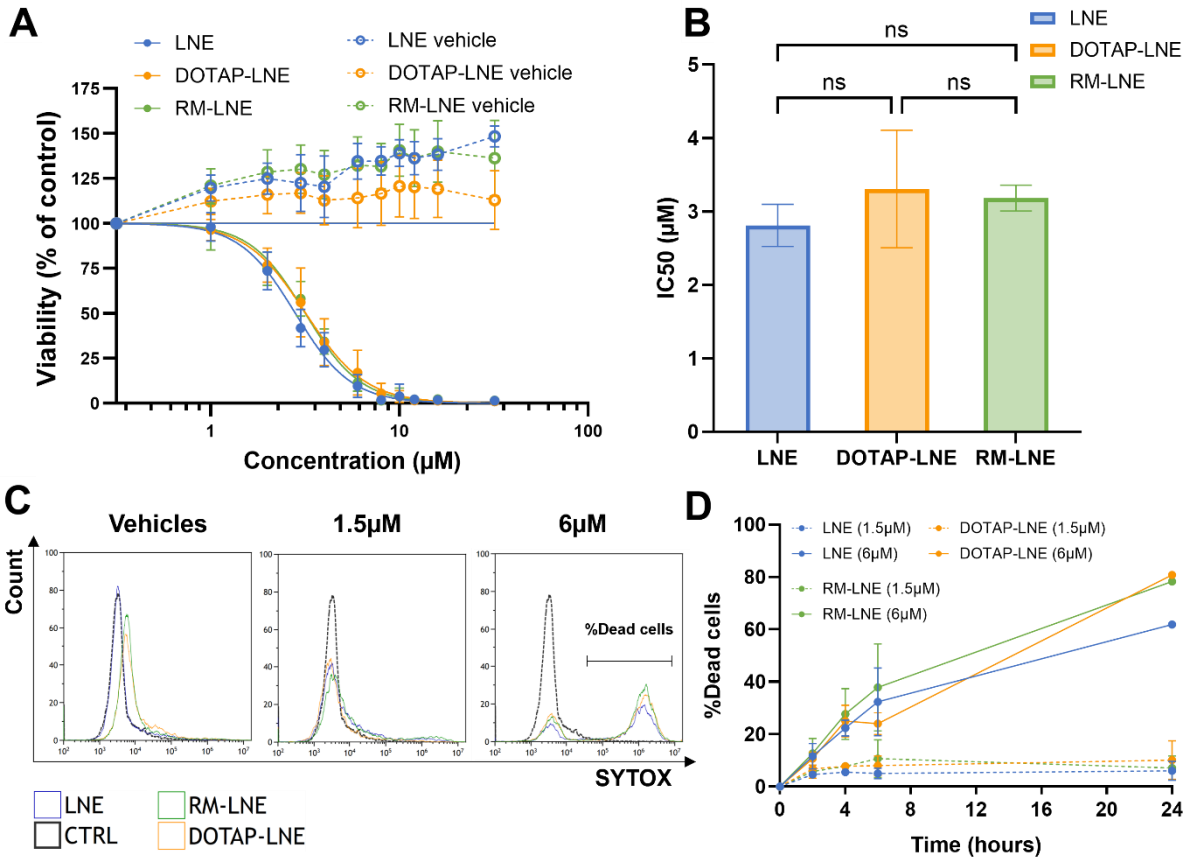

***Figure 7**: **In vitro evaluation of cytotoxicity against H358 cells for ABD0171 encapsulated in LNE, DOTAP-LNE, and DOTAP-RM-LNE formulations**. **(A)** Inhibition curves for LNE, DOTAP-LNE, and RM-LNE formulations with encapsulated ABD-0171 compared to their respective vehicles. Data are presented as mean ± SD of 15 replicates for each formulation. **(B)** IC50 values for ABD-0171 encapsulated formulations, based on the mean of three independent experiments (mean ± SD). **(C)** Flow cytometry histograms comparing the untreated control to sample treated with formulations without ABD-0171 (vehicles) and formulations encapsulating ABD-0171 at 1.5 µM and 6 µM. Cell viability was assessed by SYTOX staining, with a bar representing the dead cell population. (D) Time-dependent evolution of dead cell populations for ABD-0171 encapsulated formulations.*

***In vivo* toxicity evaluation in mice**

The *in vivo* toxicity profiles of the DOTAP-LNE formulation showed a dose-dependent toxicity. At doses ≥80 mg/kg, acute respiratory distress and mortality occurred within 24 h of post-administration. Necropsy revealed severe pulmonary edema, characterized by uniform red/purple discoloration and fluid accumulation in the lungs (**Supplementary information Figure S6)**, indicating direct pulmonary toxicity linked to the cationic lipid component. When the frequency of DOTAP-LNE administration was reduced (40 mg/kg, twice weekly over four weeks), tolerability significantly improved, with no observed respiratory distress or mortality (**Figure S5 in supplementary information**). This optimized protocol balanced safety with therapeutic dosing, highlighting the importance of adjusting treatment regimens for cationic lipid-based nanosystems.

This acute toxicity observed with DOTAP-LNE aligns with previous reports linking cationic lipids to pulmonary surfactant disruption and inflammation [47]. Additionally, the strong pulmonary tropism of DOTAP-based nanoparticles [48,49] further supports their potential for lung-targeted drug delivery. Taken together, our results demonstrate that the therapeutic benefits of ALDHin formulated as lipid nanoemulsions necessitate careful optimization of dosing regimens and administration frequencies to mitigate off-target toxicities while maintaining therapeutic efficacy.

In vivo assessment of toxicity and efficacy using the chicken CAM assay

To complement *in vivo* toxicity studies in mice, we also conducted an *in vivo* toxicity and efficacy study using a CAM assay grafted with tumors derived from the H358 cell line. This model allows for the simultaneous evaluation of compound toxicity and therapeutic potential, leveraging its ability to provide insights into tumor weight reduction and embryotoxicity. The chicken CAM assay was performed using four formulations of ABD0171 (ABD0171 free compound, LNE, DOTAP-LNE, and RM-LNE) at two dose levels (2.76 [1X] and 27.6 [10X] mg/kg). The high dose was administered once at Embryonic Development Day (EDD) 11, and the low dose was administered twice at EDD11 and EDD13. At a low dose (2.76 mg/kg [1X]), all formulations were well tolerated with embryotoxicity within the range of the NaCl0.9% control group (**Figure 8B**). In contrast, at a high dose (27.6 mg.kg [10X]), high embryotoxicity was observed, especially for the control ABD0171 free compound, limiting sample availability (n = 6) for efficacy evaluation (**Supplementary Information figure S7**). At high doses, all formulations caused severe CAM alterations, including hemorrhages, vessel coagulation, and

blood clots **(Figure 8A),** necessitating the omission of a second administration. Interestingly, yellow oily droplets were observed on tumors treated with ABD0171-DOTAP-LNE and ABD0171-RM-LNE at 27.6 mg/kg **(Supplementary information Figure S8**), suggesting possible colloidal precipitation due to the CAM environment, inducing localized release dynamics preventing from the proper distribution of the ALDHin. The low-dose groups exhibited no visible toxicity or CAM alterations **(Figure 8A)**, and two administrations were successfully delivered. Tumor weight analysis (**Figure 8C**) showed that at low dose, the ABD0171 free compound significantly reduced tumor weight by 25% compared to the untreated negative control. ABD0171-DOTAP-LNE resulted in 28% tumor regression compared to the negative control, highlighting its therapeutic potential while maintaining a manageable toxicity profile. ABD0171-RM-LNE also induced a decrease of tumor weight by 15%, although this effect was not significant compared with the untreated control.

Thus, the formulation incorporating DOTAP as reverse micelles within the oily core led to reduced tumor weight, validating its antitumor efficacy compared to the one-pot formulation, where DOTAP is assumed to be predominantly localized at the surface. The physical state of the oil core in LNE is known to be determined by the type of oil, its concentration, and the presence of stabilizing structures. Mygliol™ (caprylic/capric triglycerides) is a liquid at ambient temperature characterized by low viscosity and high fluidity, which facilitates the rapid release of encapsulated molecules [20]. However, the incorporation of structures, such as DOTAP-RM, can alter this state. Interactions between DOTAP and triglycerides can increase the local viscosity and modify the crystallinity of the lipid matrix, thus affecting overall fluidity [50,51]. For instance, AOT reverse micelles create semi-structured or semi-solid regions within the oil core Labrafac WL 1349 [14], which slows the diffusion of active molecules, resulting in more controlled release [51,52]. Furthermore, the addition of stabilizing structures can influence the migration of DOTAP from the oil core to the nanoemulsion surface. In simpler systems, such as the SORT LNPs described by Dilliard et al. [18], the low viscosity and fluidity of the lipids allowed for easy migration of DOTAP from the oil core to the surface. In contrast, in more complex and "rigid" systems, such as LNE, the increased viscosity and more ordered organization of the oily phase could hinder this migration, reducing the DOTAP concentration at the surface. In summary, the physical state of the oily core in our LNE formulation likely influences DOTAP migration and drug release by slowing or modulating its diffusion, thus reducing the therapeutic performance of the resulting formulation. However, this effect could be further modulated in more complex environments such as complete blood circulation.

The chicken CAM assay results align with the *in vivo* findings in mice, where ABD0171-DOTAP-LNE demonstrated dose-dependent toxicity, and improved tolerability and therapeutic efficacy at optimized doses compared to non-formulated ABD0171. The embryotoxicity and CAM alterations at higher doses further reinforce the necessity for dose optimization for the delivery of ALDHin using cationic lipid-based formulations. The chicken CAM assay has emerged as a promising *in vivo* platform for evaluating the therapeutic potential of nanoparticle-based anti-cancer formulations. Its rich vascularization and ability to support tumor grafts makes it particularly valuable for assessing drug distribution, tumor penetration, and formulation stability [53]. Several studies have demonstrated the effectiveness of the chicken CAM assay in evaluating the efficacy of anticancer treatments, including those aimed at targeting metastasis, while providing valuable insights into the interaction between drugs and tumor tissues [54,55]. The CAM assay offers an ethical and cost-effective alternative to traditional animal models, enabling the real-time evaluation of therapeutic responses within a dynamic and physiologically relevant environment. It has been extensively used to test various drug delivery systems, including lipid nanoparticles, liposomes, and other formulations, making it an ideal platform for assessing the performance of new anticancer therapies [53,56]. Although the chicken CAM assay does not fully replicate the human immune system, it remains a valuable tool for evaluating drug delivery efficiency, tumor targeting, and metastatic inhibition, thus playing a crucial role in the preclinical development of novel anticancer therapies [57]. Overall, it can be assumed that the promising results obtained using the CAM model will translate into mouse models, paving the way for human translation.

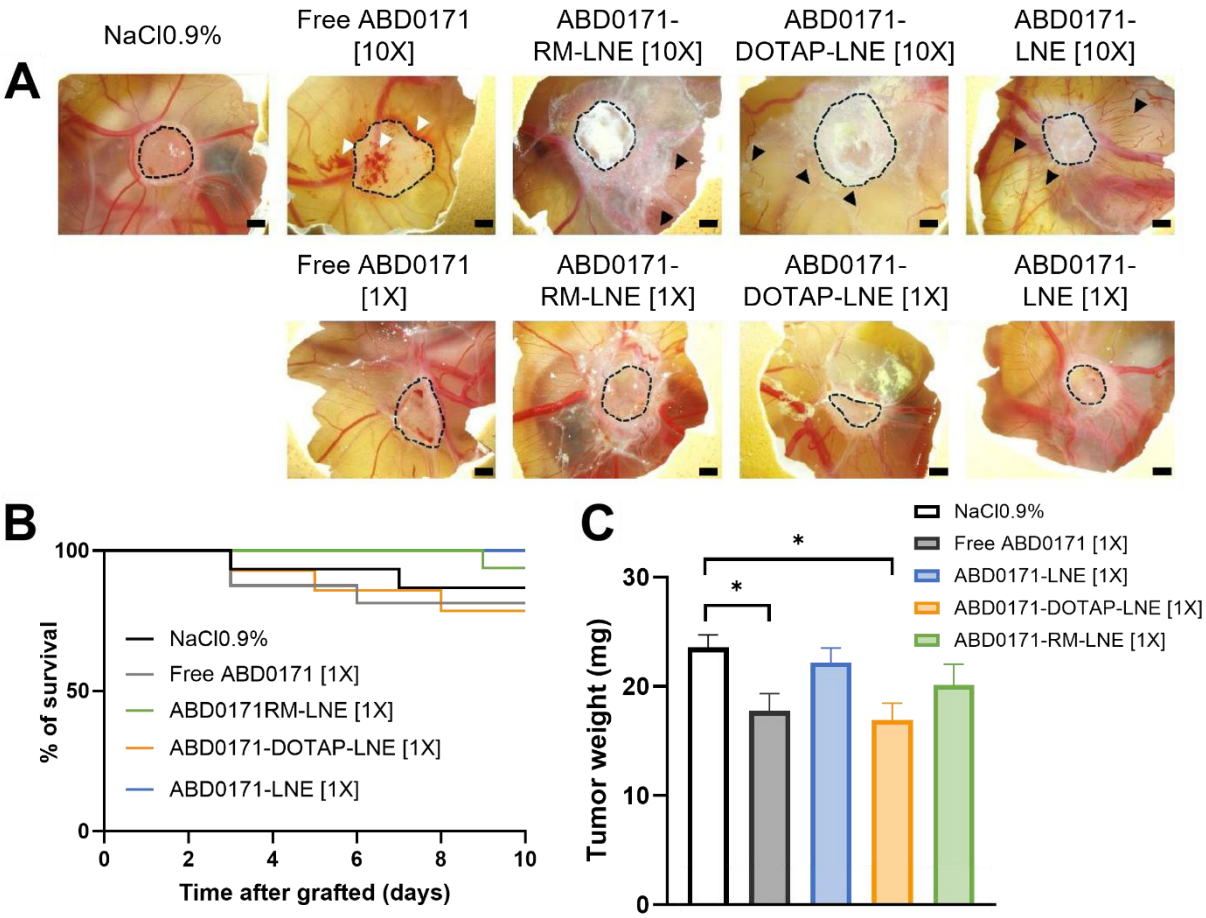

***Figure 8**: **Evaluation of toxicity and therapeutic efficacy using the chicken CAM assay**. (A) Illustrative images of the CAM 24 h after the first administration of each formulation for the two different doses ([1X] low dose of 2.76 mg/kg, [10X] high dose of 27.6 mg/kg). White arrows denote hemorrhage, whereas black arrows indicate vessel coagulation and lysis. The tumor is outlined with a black dotted line; tumor boundaries are approximate owing to challenges in visualization when the CAM is altered. Scale bar = 2 mm. (B) Kaplan-Meier survival curves for groups treated with low doses. (C) Mean tumor weight (mg) measured across the experimental groups at the end of the study with low dose.*

4. CONCLUSION

In this study, we successfully developed, optimized, and characterized lipid nanoemulsions (LNEs) incorporating DOTAP lipids, with and without reverse micelle structures. Using fluorescence spectroscopy and dynamic light scattering (DLS), we demonstrated the feasibility of forming reverse micelles (RMs) within the oily core of LNEs and validated their ability to encapsulate DOTAP, a cationic lipid known for its potential in targeted pulmonary drug delivery. We successfully encapsulated a second-generation ALDH inhibitor, ABD0171, with a high encapsulation efficiency (100%) and stability, consistent with its elevated lipophilicity and compatibility with the lipid core. Structural analyses revealed that incorporating DOTAP into the LNE systems increased the particle size and influenced the curvature parameters without compromising the stability. Positive zeta potential values were consistently observed across formulations, reflecting surface charge saturation and allowing colloidal stability of these nanoemulsions during long-term storage.

In vitro, the IC50 values of all formulations were consistently below 5 µM, indicating strong therapeutic potential against H358 NSCLC cells. Moreover, despite the presence of cationic charges in DOTAP-containing formulations, no significant toxicity was observed in the absence of ALDHin, highlighting the biocompatibility of the formulations. *In vivo* evaluation revealed dose-dependent toxicity of DOTAP-containing LNE formulations, with higher doses resulting in pulmonary toxicity in mice. This highlights the need for careful dose optimization to mitigate the adverse effects associated with cationic lipids for the delivery of ALDHin, especially in sensitive species, such as rodents. At lower doses, the DOTAP-LNE formulation showed therapeutic efficacy with manageable toxicity in the chicken CAM assay, demonstrating the possibility of fine-tuning the dosage and administration protocols for maximizing the therapeutic benefit of these formulations.

This work highlights the potential of reverse micelle-based LNEs for encapsulating lipophilic ALDH inhibitors, with DOTAP incorporation improving the stability and encapsulation efficiency of these compounds. Future studies should explore the use of reverse micelles to encapsulate hydrophilic molecules and further optimize these formulations to improve drug delivery efficiency and reduce toxicity. Overall, this study provides a solid starting point for optimizing DOTAP-containing LNEs for ALDHin delivery, positioning them as promising platforms for drug delivery in lung cancer therapy. These nanoemulsions have the potential to enter clinical trials and offer significant benefits to patients with NSCLC. These promising

results from preclinical assessments pave the way for further exploration in broader therapeutic settings, thereby establishing a promising trajectory for clinical translation.

5. ASSOCIATED CONTENT

Supporting information

6. AUTHOR INFORMATION

6.1. Corresponding authors

Alice Gaudin, alice.gaudin@a-biodesign.com; Isabelle Texier, isabelle.texier-nogues@cea.fr

6.2. Authors

Maria Irujo

6.3. Author contributions

Maria Irujo: Conceptualization, visualization, writing – original draft, writing – review and editing. Alice Gaudin: Writing – review and editing, supervision. Mileydis Perez: Writing – review and editing, supervision, funding acquisition. Isabelle Texier: Writing – review and editing, supervision.

6.4. Notes

7. ACKNOWLEDGEMENTS

This work used the platforms of the Grenoble Instruct-ERIC centre (ISBG ; UAR 3518 CNRS-CEA-UGA-EMBL) within the Grenoble Partnership for Structural Biology (PSB), supported by FRISBI (ANR-10-INBS-0005-02) and GRAL, financed within the University Grenoble Alpes graduate school (Ecoles Universitaires de Recherche) CBH-EUR-GS (ANR-17-EURE-0003). The IBS-ISBG EM facility is supported by the Auvergne-Rhône-Alpes Region, the Fondation Recherche Medicale (FRM), the fonds FEDER and the GIS-Infrastructures en Biologie Sante et Agronomie (IBISA). We thank Guy Schoehn for establishing and managing the IBS-ISBG cryo-electron microscopy platform and for providing access, training and support.

This work was supported by the French National Research Agency (ANR) through Labex ARCANE/CBH-EUR-GS program (ANR-17-EURE-0003).

8. FUNDING

This work was supported by a CIFRE fellowship from the French National Association for Research and Technology (ANRT), under grant number N° 2020/0502.

9. DISCLOSURE STATEMENT

The authors have no relevant affiliations or financial involvement with any organization or entity with a financial interest in or financial conflict with the subject matter or materials discussed in the manuscript. This includes employment, consultancies, honoraria, stock ownership or options, expert testimony, grants or patents received or pending, or royalties.
No writing assistance was utilized in the production of this manuscript.

10. REFERENCES

(1) Thai, A. A.; Solomon, B. J.; Sequist, L. V.; Gainor, J. F.; Heist, R. S. Lung Cancer. *The Lancet* **2021**, *398* (10299), 535–554. https://doi.org/10.1016/S0140-6736(21)00312-3.
(2) Abu Rous, F.; Singhi, E. K.; Sridhar, A.; Faisal, M. S.; Desai, A. Lung Cancer Treatment Advances in 2022. *Cancer Investigation* **2023**, *41* (1), 12–24. https://doi.org/10.1080/07357907.2022.2119479.
(3) Alduais, Y.; Zhang, H.; Fan, F.; Chen, J.; Chen, B. Non-Small Cell Lung Cancer (NSCLC): A Review of Risk Factors, Diagnosis, and Treatment. *Medicine* **2023**, *102* (8), e32899. https://doi.org/10.1097/MD.0000000000032899.
(4) Adams, S. J.; Stone, E.; Baldwin, D. R.; Vliegenthart, R.; Lee, P.; Fintelmann, F. J. Lung Cancer Screening. *The Lancet* **2023**, *401* (10374), 390–408. https://doi.org/10.1016/S0140-6736(22)01694-4.
(5) Wang, J.; Zhou, T.; Liu, Y.; Chen, S.; Yu, Z. Application of Nanoparticles in the Treatment of Lung Cancer With Emphasis on Receptors. *Front. Pharmacol.* **2022**, *12*, 781425. https://doi.org/10.3389/fphar.2021.781425.
(6) Rebollido-Rios, R.; Venton, G.; Sánchez-Redondo, S.; Iglesias i Felip, C.; Fournet, G.; González, E.; Romero Fernández, W.; Borroto Escuela, D. O.; Di Stefano, B.; Penarroche-Díaz, R.; Martin, G.; Ceylan, I.; Costello, R.; Perez-Alea, M. Dual Disruption of Aldehyde Dehydrogenases 1 and 3 Promotes Functional Changes in the Glutathione Redox System and Enhances Chemosensitivity in Nonsmall Cell Lung Cancer. *Oncogene* **2020**, *39* (13), 2756–2771. https://doi.org/10.1038/s41388-020-1184-9.
(7) Prabavathy, D.; Swarnalatha, Y.; Ramadoss, N. Lung Cancer Stem Cells-Origin, Characteristics and Therapy. *Stem Cell Investig* **2018**, *5*, 6. https://doi.org/10.21037/sci.2018.02.01.
(8) Li, X.; Wan, L.; Geng, J.; Wu, C.-L.; Bai, X. Aldehyde Dehydrogenase 1A1 Possesses Stem-Like Properties and Predicts Lung Cancer Patient Outcome. *Journal of Thoracic Oncology* **2012**, *7* (8), 1235–1245. https://doi.org/10.1097/JTO.0b013e318257cc6d.

(9) Layek, B.; Gidwani, B.; Tiwari, S.; Joshi, V.; Jain, V.; Vyas, A. Recent Advances in Lipid-Based Nanodrug Delivery Systems in Cancer Therapy. *CPD* **2020**, *26* (27), 3218–3233. https://doi.org/10.2174/1381612826666200622133407.
(10) Omidian, H.; Gill, E. J.; Cubeddu, L. X. Lipid Nanoparticles in Lung Cancer Therapy. *Pharmaceutics* **2024**, *16* (5), 644. https://doi.org/10.3390/pharmaceutics16050644.
(11) Apostolou, M.; Fatokun, A. A.; Assi, S.; Khan, I. Targeted Lipid-Based Drug Delivery Systems for Lung Cancer Therapy. *Applied Sciences* **2024**, *14* (15), 6759. https://doi.org/10.3390/app14156759.
(12) Vrignaud, S.; Anton, N.; Gayet, P.; Benoit, J.-P.; Saulnier, P. Reverse Micelle-Loaded Lipid Nanocarriers: A Novel Drug Delivery System for the Sustained Release of Doxorubicin Hydrochloride. *European Journal of Pharmaceutics and Biopharmaceutics* **2011**, *79* (1), 197–204. https://doi.org/10.1016/j.ejpb.2011.02.015.
(13) Vrignaud, S.; Hureaux, J.; Wack, S.; Benoit, J.-P.; Saulnier, P. Design, Optimization and in Vitro Evaluation of Reverse Micelle-Loaded Lipid Nanocarriers Containing Erlotinib Hydrochloride. *International Journal of Pharmaceutics* **2012**, *436* (1–2), 194–200. https://doi.org/10.1016/j.ijpharm.2012.06.026.
(14) Groo, A.-C.; Matougui, N.; Umerska, A.; Saulnier, P. Reverse Micelle-Lipid Nanocapsules: A Novel Strategy for Drug Delivery of the Plectasin Derivate AP138 Antimicrobial Peptide. *IJN* **2018**, *Volume 13*, 7565–7574. https://doi.org/10.2147/IJN.S180040.
(15) Li, S.-D.; Huang, L. Nanoparticles Evading the Reticuloendothelial System: Role of the Supported Bilayer. *Biochimica et Biophysica Acta (BBA) - Biomembranes* **2009**, *1788* (10), 2259–2266. https://doi.org/10.1016/j.bbamem.2009.06.022.
(16) Rosenblum, D.; Joshi, N.; Tao, W.; Karp, J. M.; Peer, D. Progress and Challenges towards Targeted Delivery of Cancer Therapeutics. *Nat Commun* **2018**, *9* (1), 1410. https://doi.org/10.1038/s41467-018-03705-y.
(17) Dilliard, S. A.; Siegwart, D. J. Passive, Active and Endogenous Organ-Targeted Lipid and Polymer Nanoparticles for Delivery of Genetic Drugs. *Nat Rev Mater* **2023**, *8* (4), 282–300. https://doi.org/10.1038/s41578-022-00529-7.
(18) Dilliard, S. A.; Cheng, Q.; Siegwart, D. J. On the Mechanism of Tissue-Specific mRNA Delivery by Selective Organ Targeting Nanoparticles. *Proc. Natl. Acad. Sci. U.S.A.* **2021**, *118* (52), e2109256118. https://doi.org/10.1073/pnas.2109256118.
(19) Pequerul, R.; Constantinescu, A.; Janji, B.; Kumar, A.; Parés, X.; Palacios, O.; Colignon, D.; Berrou, A.; Fournet, G.; Berchard, P.; Martin, G.; Ceylan, I.; Rebollido-Ríos, R.; Farrés, J.; Perez-Alea, M. ALDH1 Subtype-Specific Inhibitor Targets Key Cancerous Epithelial Cell Populations in Aggressive Subtypes of Breast Cancer. October 22, 2024. https://doi.org/10.1101/2024.10.18.619128.
(20) Heurtault, B.; Saulnier, P.; Pech, B.; Proust, J.; Benoit, J. A Novel Phase Inversion-Based Process for the Preparation of Lipid Nanocarriers. *Pharmaceutical Research* **2002**, *19* (6), 875–880. https://doi.org/10.1023/A:1016121319668.
(21) Garcion, E. A New Generation of Anticancer, Drug-Loaded, Colloidal Vectors Reverses Multidrug Resistance in Glioma and Reduces Tumor Progression in Rats. *Molecular Cancer Therapeutics* **2006**, *5* (7), 1710–1722. https://doi.org/10.1158/1535-7163.MCT-06-0289.
(22) He, J.; Ding, R.; Tao, Y.; Zhao, Z.; Yuan, R.; Zhang, H.; Wang, A.; Sun, K.; Li, Y.; Shi, Y. Folic Acid-Modified Reverse Micelle-Lipid Nanocapsules Overcome Intestinal Barriers and Improve the Oral Delivery of Peptides. *Drug Delivery* **2023**, *30* (1), 2181744. https://doi.org/10.1080/10717544.2023.2181744.
(23) Jörgensen, A. M.; Steinbring, C.; Stengel, D.; To, D.; Schmid, P.; Bernkop-Schnürch, A. Self-Emulsifying Drug Delivery Systems (SEDDS) Containing Reverse Micelles: Advanced Oral Formulations for Therapeutic Peptides. *Adv Healthcare Materials* **2023**, *12* (31), 2302034. https://doi.org/10.1002/adhm.202302034.

(24) Bohidar, H. B.; Behboudnia, M. Characterization of Reverse Micelles by Dynamic Light Scattering. *Colloids and Surfaces A: Physicochemical and Engineering Aspects* **2001**, *178* (1–3), 313–323. https://doi.org/10.1016/S0927-7757(00)00736-6.
(25) Chen, R. F.; Knutson, J. R. Mechanism of Fluorescence Concentration Quenching of Carboxyfluorescein in Liposomes: Energy Transfer to Nonfluorescent Dimers. *Analytical Biochemistry* **1988**, *172* (1), 61–77. https://doi.org/10.1016/0003-2697(88)90412-5.
(26) Anton, N.; Mojzisova, H.; Porcher, E.; Benoit, J.-P.; Saulnier, P. Reverse Micelle-Loaded Lipid Nano-Emulsions: New Technology for Nano-Encapsulation of Hydrophilic Materials. *International Journal of Pharmaceutics* **2010**, *398* (1–2), 204–209. https://doi.org/10.1016/j.ijpharm.2010.07.039.
(27) Pavoni, L.; Perinelli, D. R.; Ciacciarelli, A.; Quassinti, L.; Bramucci, M.; Miano, A.; Casettari, L.; Cespi, M.; Bonacucina, G.; Palmieri, G. F. Properties and Stability of Nanoemulsions: How Relevant Is the Type of Surfactant? *Journal of Drug Delivery Science and Technology* **2020**, *58*, 101772. https://doi.org/10.1016/j.jddst.2020.101772.
(28) Schubert, M. A.; Müller-Goymann, C. C. Characterisation of Surface-Modified Solid Lipid Nanoparticles (SLN): Influence of Lecithin and Nonionic Emulsifier. *European Journal of Pharmaceutics and Biopharmaceutics* **2005**, *61* (1–2), 77–86. https://doi.org/10.1016/j.ejpb.2005.03.006.
(29) *Intermolecular and Surface Forces*; Elsevier, 2011. https://doi.org/10.1016/C2009-0-21560-1.
(30) Goyal, P. S.; Aswal, V. K. Micellar Structure and Inter-Micelle Interactions in Micellar Solutions: Results of Small Angle Neutron Scattering Studies. *Current Science* **2001**, *80* (8), 972–979.
(31) Stewart, P. L. Cryo-electron Microscopy and Cryo-electron Tomography of Nanoparticles. *WIREs Nanomed Nanobiotechnol* **2017**, *9* (2), e1417. https://doi.org/10.1002/wnan.1417.
(32) Hunter, R. J.; Ottewill, R. H.; Rowell, R. L. *Zeta Potential in Colloid Science: Principles and Applications*; Elsevier Science: Burlington, 1981.
(33) Smith, M. C.; Crist, R. M.; Clogston, J. D.; McNeil, S. E. Zeta Potential: A Case Study of Cationic, Anionic, and Neutral Liposomes. *Anal Bioanal Chem* **2017**, *409* (24), 5779–5787. https://doi.org/10.1007/s00216-017-0527-z.
(34) Wang, L.; Xing, H.; Guo, S.; Cao, W.; Zhang, Z.; Huang, L.; Xin, S.; Luo, Y.; Wang, Y.; Yang, J. Negatively Charged Phospholipids Doped Liposome Delivery System for mRNA with High Transfection Efficiency and Low Cytotoxicity. *Drug Delivery* **2023**, *30* (1), 2219869. https://doi.org/10.1080/10717544.2023.2219869.
(35) Hou, X.; Zaks, T.; Langer, R.; Dong, Y. Lipid Nanoparticles for mRNA Delivery. *Nat Rev Mater* **2021**, *6* (12), 1078–1094. https://doi.org/10.1038/s41578-021-00358-0.
(36) Roger, E.; Franconi, F.; Do, T. A. T.; Simonsson, C.; Siegler, B.; Perrot, R.; Saulnier, P.; Gimel, J.-C. Evidence of Residual Micellar Structures in a Lipid Nanocapsule Dispersion. A Multi-Technique Approach. *Journal of Controlled Release* **2023**, *364*, 700–717. https://doi.org/10.1016/j.jconrel.2023.10.054.
(37) Yegin, B.; Lamprecht, A. Lipid Nanocapsule Size Analysis by Hydrodynamic Chromatography and Photon Correlation Spectroscopy. *International Journal of Pharmaceutics* **2006**, *320* (1–2), 165–170. https://doi.org/10.1016/j.ijpharm.2006.04.014.
(38) Knoke, S.; Bunjes, H. Transfer of Lipophilic Drugs from Nanoemulsions into Lipid-Containing Alginate Microspheres. *Pharmaceutics* **2021**, *13* (2), 173. https://doi.org/10.3390/pharmaceutics13020173.
(39) Spinozzi, F.; Moretti, P.; Perinelli, D. R.; Corucci, G.; Piergiovanni, P.; Amenitsch, H.; Sancini, G. A.; Franzese, G.; Blasi, P. Small-Angle X-Ray Scattering Unveils the Internal Structure of Lipid Nanoparticles. *Journal of Colloid and Interface Science* **2024**, *662*, 446–459. https://doi.org/10.1016/j.jcis.2024.02.076.
(40) Danaei, M.; Dehghankhold, M.; Ataei, S.; Hasanzadeh Davarani, F.; Javanmard, R.; Dokhani, A.; Khorasani, S.; Mozafari, M. R. Impact of Particle Size and Polydispersity Index

on the Clinical Applications of Lipidic Nanocarrier Systems. *Pharmaceutics* **2018**, *10* (2), 57. https://doi.org/10.3390/pharmaceutics10020057.
(41) Goldstein, M. J.; Peters, M.; Weber, B. L.; Davis, C. B. Optimizing the Therapeutic Window of Targeted Drugs in Oncology: Potency-Guided First-in-Human Studies. *Clinical Translational Sci* **2021**, *14* (2), 536–543. https://doi.org/10.1111/cts.12902.
(42) Sharma, S.; Parveen, R.; Chatterji, B. P. Toxicology of Nanoparticles in Drug Delivery. *Curr Pathobiol Rep* **2021**, *9* (4), 133–144. https://doi.org/10.1007/s40139-021-00227-z.
(43) Van Meer, G.; Voelker, D. R.; Feigenson, G. W. Membrane Lipids: Where They Are and How They Behave. *Nat Rev Mol Cell Biol* **2008**, *9* (2), 112–124. https://doi.org/10.1038/nrm2330.
(44) Green, D. E.; Tzagoloff, A. Role of Lipids in the Structure and Function of Biological Membranes. *J Lipid Res* **1966**, *7* (5), 587–602.
(45) Luo, X.; Cheng, C.; Tan, Z.; Li, N.; Tang, M.; Yang, L.; Cao, Y. Emerging Roles of Lipid Metabolism in Cancer Metastasis. *Mol Cancer* **2017**, *16* (1), 76. https://doi.org/10.1186/s12943-017-0646-3.
(46) Salatin, S.; Maleki Dizaj, S.; Yari Khosroushahi, A. Effect of the Surface Modification, Size, and Shape on Cellular Uptake of Nanoparticles. *Cell Biology International* **2015**, *39* (8), 881–890. https://doi.org/10.1002/cbin.10459.
(47) Skovgaard Poulsen, H.; Arildsen; Roth, J.; Skovgaard Poulsen, H.; Tuxen Poulsen; Christensen; Handlos; Gjetting, T. In Vitro and in Vivo Effects of Polyethylene Glycol (PEG)-Modified Lipid in DOTAP/Cholesterol-Mediated Gene Transfection. *IJN* **2010**, 371. https://doi.org/10.2147/IJN.S10462.
(48) Omo-Lamai, S.; Zamora, M. E.; Patel, M. N.; Wu, J.; Nong, J.; Wang, Z.; Peshkova, A.; Chase, L. S.; Essien, E.-O.; Muzykantov, V.; Marcos-Contreras, O.; Myerson, J. W.; Brenner, J. S. Physicochemical Targeting of Lipid Nanoparticles to the Lungs Induces Clotting: Mechanisms and Solutions. *bioRxiv* **2023**, 2023.07.21.550080. https://doi.org/10.1101/2023.07.21.550080.
(49) Sun, H.; Zhang, Y.; Wang, J.; Su, J.; Zhou, D.; Yu, X.; Xu, Y.; Yang, W. Application of Lung-Targeted Lipid Nanoparticle-Delivered mRNA of Soluble PD-L1 via SORT Technology in Acute Respiratory Distress Syndrome. *Theranostics* **2023**, *13* (14), 4974–4992. https://doi.org/10.7150/thno.86466.
(50) Delmas, T.; Couffin, A.-C.; Bayle, P. A.; de Crécy, F.; Neumann, E.; Vinet, F.; Bardet, M.; Bibette, J.; Texier, I. Preparation and Characterization of Highly Stable Lipid Nanoparticles with Amorphous Core of Tuneable Viscosity. *J Colloid Interface Sci* **2011**, *360* (2), 471–481. https://doi.org/10.1016/j.jcis.2011.04.080.
(51) Peltier, S.; Oger, J.-M.; Lagarce, F.; Couet, W.; Benoît, J.-P. Enhanced Oral Paclitaxel Bioavailability After Administration of Paclitaxel-Loaded Lipid Nanocapsules. *Pharm Res* **2006**, *23* (6), 1243–1250. https://doi.org/10.1007/s11095-006-0022-2.
(52) Gravier, J.; Navarro, F. P.; Delmas, T.; Mittler, F.; Couffin, A.-C.; Vinet, F.; Texier, I. Lipidots: Competitive Organic Alternative to Quantum Dots for in Vivo Fluorescence Imaging. *J. Biomed. Opt.* **2011**, *16* (9), 096013. https://doi.org/10.1117/1.3625405.
(53) Schneider-Stock, R.; Ribatti, D. The CAM Assay as an Alternative In Vivo Model for Drug Testing. In *Organotypic Models in Drug Development*; Schäfer-Korting, M., Stuchi Maria-Engler, S., Landsiedel, R., Eds.; Handbook of Experimental Pharmacology; Springer International Publishing: Cham, 2020; Vol. 265, pp 303–323. https://doi.org/10.1007/164_2020_375.
(54) Pawlikowska, P.; Tayoun, T.; Oulhen, M.; Faugeroux, V.; Rouffiac, V.; Aberlenc, A.; Pommier, A. L.; Honore, A.; Marty, V.; Bawa, O.; Lacroix, L.; Scoazec, J. Y.; Chauchereau, A.; Laplace-Builhe, C.; Farace, F. Exploitation of the Chick Embryo Chorioallantoic Membrane (CAM) as a Platform for Anti-Metastatic Drug Testing. *Sci Rep* **2020**, *10* (1), 16876. https://doi.org/10.1038/s41598-020-73632-w.
(55) Vu, B. T.; Shahin, S. A.; Croissant, J.; Fatieiev, Y.; Matsumoto, K.; Le-Hoang Doan, T.; Yik, T.; Simargi, S.; Conteras, A.; Ratliff, L.; Jimenez, C. M.; Raehm, L.; Khashab, N.; Durand, J.-O.;

Glackin, C.; Tamanoi, F. Chick Chorioallantoic Membrane Assay as an in Vivo Model to Study the Effect of Nanoparticle-Based Anticancer Drugs in Ovarian Cancer. *Sci Rep* **2018**, *8* (1), 8524. https://doi.org/10.1038/s41598-018-25573-8.

(56) Victorelli, F. D.; Cardoso, V. M. D. O.; Ferreira, N. N.; Calixto, G. M. F.; Fontana, C. R.; Baltazar, F.; Gremião, M. P. D.; Chorilli, M. Chick Embryo Chorioallantoic Membrane as a Suitable in Vivo Model to Evaluate Drug Delivery Systems for Cancer Treatment: A Review. *European Journal of Pharmaceutics and Biopharmaceutics* **2020**, *153*, 273–284. https://doi.org/10.1016/j.ejpb.2020.06.010.

(57) Fraguas-Sánchez, A. I.; Martín-Sabroso, C.; Torres-Suárez, A. I. The Chick Embryo Chorioallantoic Membrane Model: A ResearchApproach for Ex Vivo and In Vivo Experiments. *CMC* **2022**, *29* (10), 1702–1717. https://doi.org/10.2174/0929867328666210625105438.